ELSEVIER

Earth and Planetary Science Letters 169 (1999) 147–163

EPSL

Wetting of mantle olivine by sulfide melt: implications for Re/Os ratios in mantle peridotite and late-stage core formation

Glenn A. Gaetani *, Timothy L. Grove

Department of Earth, Atmospheric, and Planetary Sciences, Massachusetts Institute of Technology, Cambridge, MA 02139, USA

Received 21 July 1998; revised version received 19 February 1999; accepted 8 March 1999

Abstract

This study investigates the effects of variations in the relative fugacities of oxygen and sulfur on the wetting of mantle olivine by molten sulfide. Experiments were performed on mixtures of San Carlos olivine and synthetic FeS at 1 bar and 1350ºC. Crucibles were fabricated from San Carlos olivine, and the fugacities of oxygen and sulfur were controlled by mixing CO_2, CO, and SO_2 gases. Experimental conditions ranged from log $f_{O_2} = -7.9$ to -10.3 and from log $f_{S_2} = -1.5$ to -2.5. Our experimental results demonstrate that, at a given temperature and pressure, the olivine–sulfide melt dihedral angle is controlled by the concentration of O dissolved in an anion-rich melt. Trace amounts of O dissolve in sulfide melt at f_{O_2} conditions near the iron–wüstite oxygen buffer and the dihedral angle is 90º. At f_{O_2} conditions near the fayalite–magnetite–quartz oxygen buffer the concentration of dissolved O is near 9 wt% and the dihedral angle is 52º, allowing small amounts of sulfide melt to form an interconnected network in olivine-rich rocks and to migrate via porous flow. These results indicate that sulfide melt is likely to be mobile at current upper mantle f_{O_2} and f_{S_2} conditions. In mantle peridotite, the addition or removal of sulfide melt by porous flow will variably fractionate Re/Os, U/Pb, and Th/Pb ratios because Os and Pb are more chalcophile than Re, U, and Th. The Re/Os ratio of the peridotite is especially sensitive to this process. The mobility of sulfide melt at oxidizing conditions implies that the addition of oxidized chondritic material during the later stages of the accretion of the Earth may have facilitated the segregation of core-forming material by porous flow if temperatures were in excess of the sulfide solidus.

Keywords: olivine; sulfides; melts; Re/Os; core

1. Introduction

Under hydrostatic conditions, the distribution and connectivity of a small amount of melt in a polycrystalline aggregate depends on the relative free energies associated with solid–melt and solid–solid interfaces. The ratio of the interfacial energies where two contacting solid grains bound a pocket of melt produces a characteristic angle (dihedral angle) that governs the amount of melt necessary to achieve connectivity. At large dihedral angles, a small amount of melt will form isolated pockets at four grain junctions if the surface energy of the solid is isotropic. As the dihedral angle decreases, however, the tendency for the melt to wet three-grain junctions increases until, at a dihedral angle of 60º or less, an interconnected network is formed even for very small melt fractions [1,2].

* Corresponding author. Present address: Department of Earth and Environmental Sciences, Rensselaer Polytechnic Institute, Troy, NY 12180, USA. Fax: +1 518 276 8627.

0012-821X/99/$ – see front matter
PII: S0012-821X(99)00062-X

Sulfide is a common phase in basalts [3–5], upper mantle xenoliths [6], and Alpine-type peridotites [7,8], and partitioning studies indicate that sulfide melt is an important repository for siderophile elements in the Earth's upper mantle [9–12]. Furthermore, molten FeNi sulfide is thought to have been one of the principle phases that segregated from the silicate portion of the early Earth to form the core, influencing the siderophile element abundances of the mantle [13–16]. Despite the importance of sulfide melt for controlling the geochemical behavior of siderophile elements in the Earth's mantle, relatively little is known about thermodynamic controls on its distribution in mantle peridotite.

Experimental determinations of dihedral angles in olivine–sulfide melt systems have thus far been restricted to conditions more reducing than are appropriate for the present day upper mantle [17–19]. One of the conclusions drawn from these studies is that anion-poor sulfide melt (anion/cation < 1) does not wet mantle olivine, but that increasing the anion content of the liquid produces a systematic decrease in the olivine–sulfide melt dihedral angle [17]. Here we present experiments performed on aggregates of mantle olivine and sulfide melt over a range of oxygen and sulfur fugacity conditions. The experimental results demonstrate that, for anion-rich sulfide melt (anion/cation > 1), the concentration of dissolved oxygen represents a primary control on olivine–sulfide melt dihedral angles. Given reasonable estimates for current upper mantle f_{O_2} and f_{S_2} conditions, sulfide melt is likely to contain several weight percent dissolved oxygen and to form an interconnected network in olivine-rich rocks, even at very low melt fractions. Percolation of sulfide melt provides a mechanism for redistributing siderophile elements in the Earth's upper mantle and for producing some of the heterogeneity observed in upper mantle materials.

2. Experimental and analytical methods

Experiments were performed in a vertical gas mixing furnace at 1 bar and 1350ºC, with f_{O_2} and f_{S_2} controlled by mixing CO_2, CO, and SO_2 gases. Experimental conditions and durations are listed in Table 1, and the combinations of f_{O_2} and f_{S_2} at which experiments were performed are shown in Fig. 1. The gas mixture required for each experiment was calculated using the method described by Gaetani and Grove [12] and is reported in Table 1. Precipitation of graphite and sulfur from the gas at the cold ends of the furnace was minimized by fabricating end pieces from fired pyrophyllite and attaching them to the muffle tube using a high-temperature silicone rubber adhesive sealant, obviating the need for cooling water. Temperature in the furnace hot spot was continuously monitored using a $Pt–Pt_{90}Rh_{10}$ thermocouple calibrated against the melting points of NaCl, Au, and Pd on the 1968 International Practical Temperature Scale [20]. The thermocouple was positioned on the outside of the muffle tube to avoid contamination by S-rich gases. A second thermocouple was used to determine a temperature difference of 8ºC between the position of the thermocouple and

Table 1
Experimental conditions and gas mixing proportions

Experiment	Duration (h)	log f_{O_2}	log f_{S_2}	Gas flow rates (ml/s) $CO_2 : CO : SO_2$
FeS-4	24	−10.3	−1.5	0.08 : 1.44 : 0.12
FeS-7	72	−10.3	−1.5	0.08 : 1.44 : 0.12
FeS-1	120	−10.3	−1.5	0.08 : 1.44 : 0.12
FeS-3	216	−10.3	−1.5	0.08 : 1.44 : 0.12
FeS-14	72	−9.5	−1.5	0.37 : 1.12 : 0.12
FeS-9	72	−8.6	−1.5	0.73 : 0.72 : 0.15
FeS-13	72	−7.9	−1.6	0.89 : 0.42 : 0.29
FeS-6	72	−7.9	−2.5	1.53 : 0.41 : 0.11

All experiments were carried out at 1350ºC. Fugacities were calculated from gas mixing proportions using the method described by Gaetani and Grove [12].

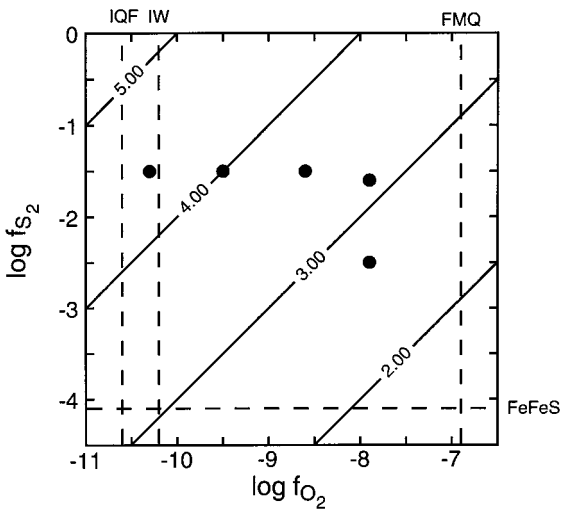

Fig. 1. Plot of log f_{S_2} vs. log f_{O_2} showing the conditions at which dihedral angle experiments were performed (filled circles). Diagonal solid lines are constant log $f_{s_2}^{1/2}$ − log $f_{O_2}^{1/2}$ contours, which is a measure of the f_{S_2}/f_{O_2} ratio derived from the equilibrium constant for reaction 5 [12]. Vertical dashed lines represent the iron–quartz–fayalite (IQF), iron–wüstite (IW), and fayalite–magnetite–quartz (FMQ) oxygen buffers at 1350ºC and 1 bar. Horizontal dashed line represents the iron–iron sulfide (FeFeS) sulfur buffer 1350ºC and 1 bar.

the position of the sample. This correction has been applied to reported temperatures. Additional details of the experimental procedures used in this study are given by Gaetani and Grove [12].

Crucibles were fabricated from San Carlos olivine ($Fo_{90.6}$) following the method described by Ehlers et al. [21]. Olivine crucibles are ideal containers for these experiments because they are inert with respect to both the experimental charge and the furnace gases. The starting material consisted of a mixture of 30 wt% synthetic FeS and 70 wt% natural San Carlos olivine. The FeS was synthesized using the method described by Gaetani and Grove [12]. Fresh, clean pieces of San Carlos olivine were hand picked, crushed, then ground to a fine powder. The appropriate amount of each powder was weighed out, then the mixture was ground by hand under ethanol for 10–20 minutes.

The compositions of experimental products were determined using a 5-spectrometer JEOL 733 electron microprobe at the Massachusetts Institute of Technology and are reported in Tables 2 and 3. Analytical conditions for determination of the major elements in all phases were an accelerating voltage of 15 kV and a beam current of 10 nA with maximum peak counting times of 40 s. A 2 μm spot size was used for olivine analyses, while a 10 μm spot was used to perform sulfide analyses. Data reduction was accomplished using the phi–rho–z correction procedure.

Accurate determination of the composition of experimentally produced sulfide melt is complicated by the presence of intergrown quench phases [9,12,22,23]. Quench growth is minimal in melts with low concentrations of O, but becomes more pronounced in experiments performed at higher f_{O_2}/f_{S_2} ratio conditions. The electron microprobe analyses presented in Table 2 were obtained from the inner portions of the charge where the sulfide contains little or no quench growth. This was done in order to minimize the possibility that the composition of the analyzed sulfide had been modified during the

Table 2
Electron microprobe analyses of experimentally produced sulfide melts

Experiment	*n*	Fe	Ni	Mn	Cr	S	O	Total
FeS-4	8	61.9 (4)	0.43 (2)	0.04 (1)	0.09 (1)	36.7 (5)	–	99.16
FeS-7	7	60.5 (10)	0.61 (9)	0.04 (1)	0.08 (1)	38.2 (7)	–	99.43
FeS-1	10	60.7 (9)	0.72 (8)	0.09 (1)	0.03 (1)	38.3 (7)	–	99.84
FeS-3	10	62.6 (4)	0.64 (7)	0.05 (1)	0.10 (1)	36.7 (2)	–	100.09
FeS-14	14	62.6 (6)	0.76 (7)	0.05 (1)	0.08 (1)	37.5 (7)	0.09 (3)	101.08
FeS-9	10	61.0 (6)	0.77 (6)	0.02 (1)	0.05 (1)	37.6 (3)	0.34 (15)	99.78
FeS-13	5	58.4 (6)	1.3 (3)	0.00 (0)	0.07 (1)	37.4 (12)	2.7 (8)	99.87
FeS-6	6	65.6 (9)	0.81 (12)	0.00 (0)	0.09 (1)	25.8 (12)	8.6 (6)	100.90

Analyses are reported in weight percent. *n* = number of analyses used to calculate the mean. Units in parentheses represent one standard deviation of least units cited, on the basis of replicate analyses. Therefore, 61.9 (4) should be read 61.9 ± 0.4.

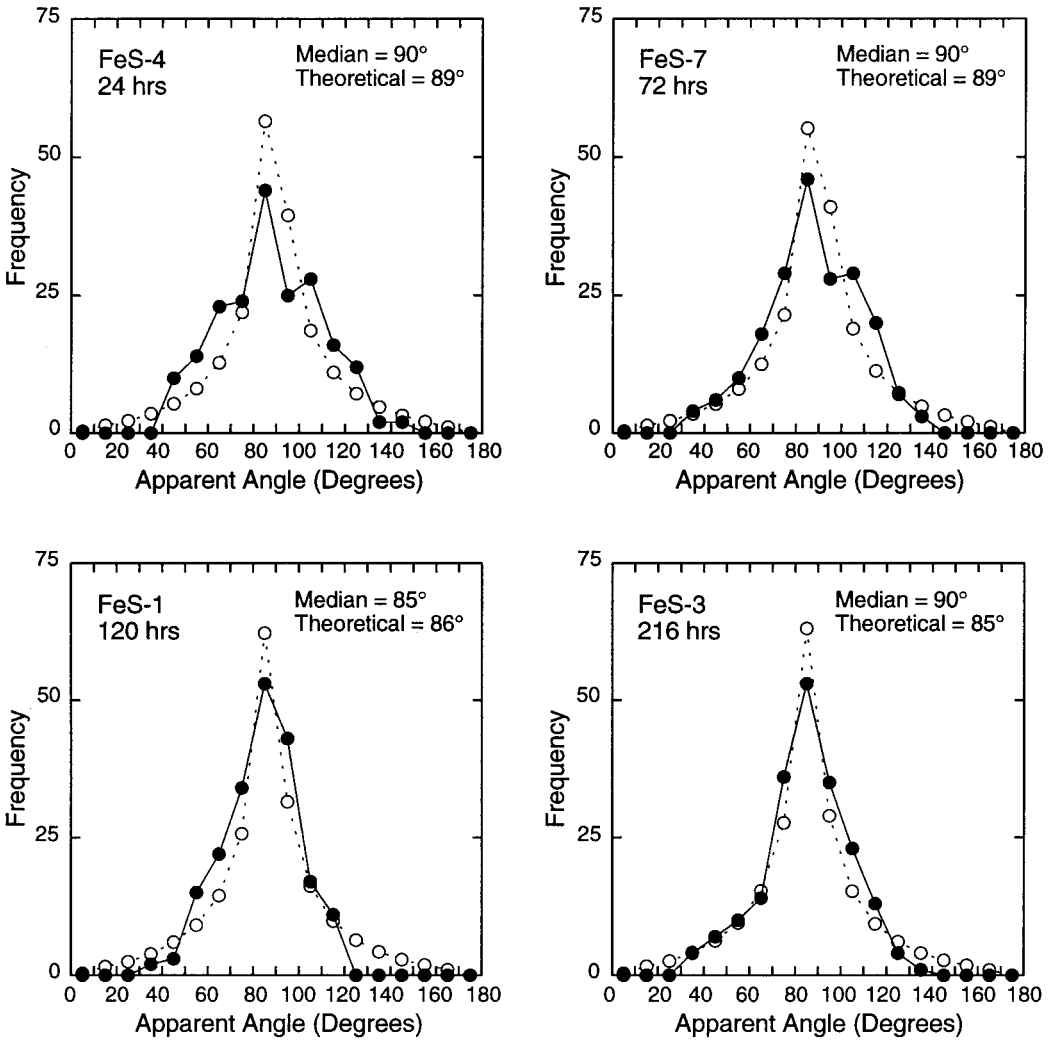

Fig. 2. Comparisons of measured (filled circles) and theoretical (open circles) frequency distributions for 200 olivine–sulfide melt apparent angles from variable duration experiments carried out at $\log f_{O_2} = -10.3$, $\log f_{S_2} = -1.5$, and 1350ºC. Theoretical distributions were calculated using the method of Harker and Parker [25], and the best match between theoretical and observed distributions was determined by minimizing χ^2. Bin size is 10º.

quench. While this precaution does not guarantee that the reported compositions are pristine, the systematic relationship between the melt compositions and the f_{S_2} and f_{O_2} conditions of the experiments indicates that compositional modification during the quench was probably not significant.

Olivine–sulfide melt dihedral angles were determined for each experiment from the distribution of 200 apparent angles measured using a protractor on reverse-polarity SEM images at a magnification of 3600 (Figs. 2 and 3). Individual apparent angle measurements for each experiment are given by Gaetani [24]. The uncertainty associated with an individual measurement is estimated to be ±5º on the basis of replicate measurements. The median angle from each distribution was taken to represent the true dihedral angle [25], and the associated uncertainty was calculated using the method of Riegger and Van Vlack [26] (Table 4). Olivine surface energy anisotropy tends to broaden the measured distribution of angles

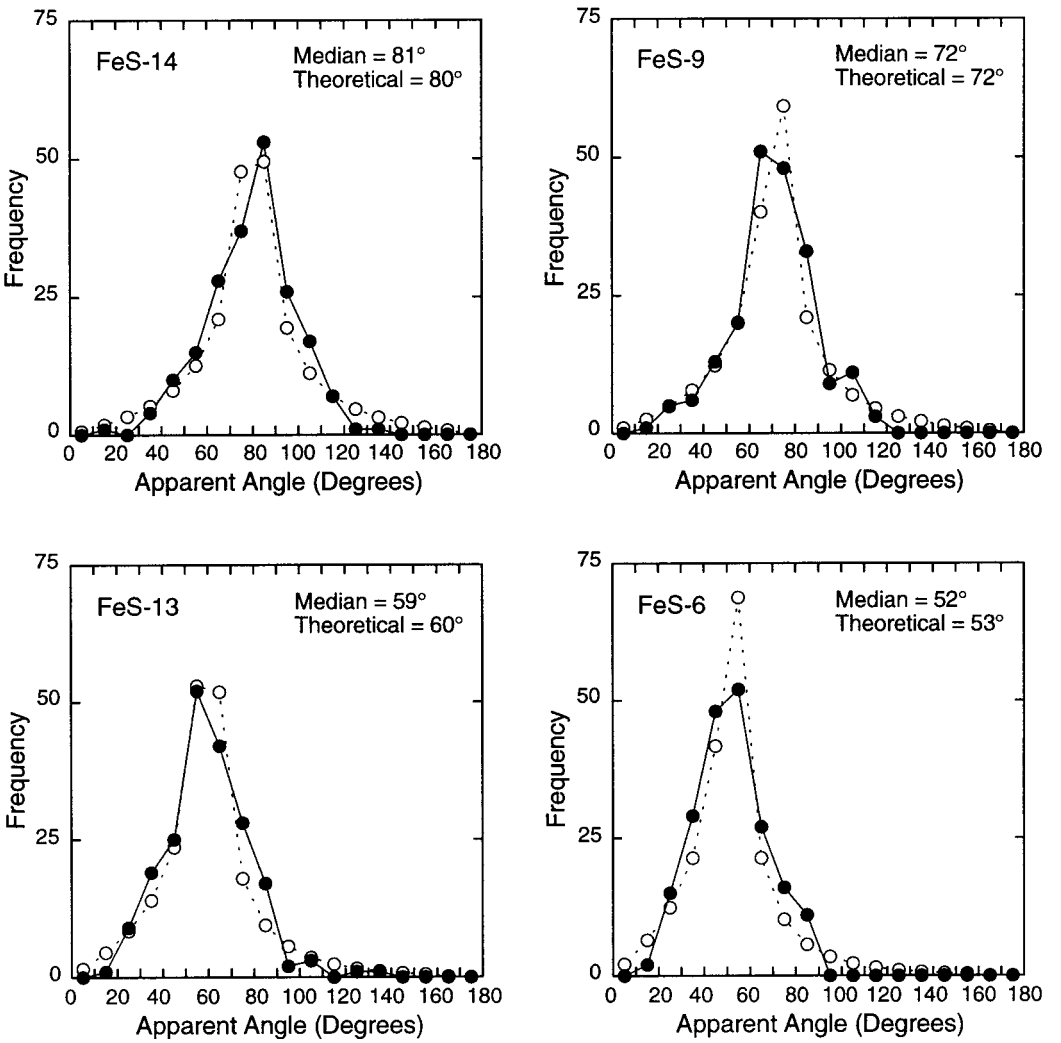

Fig. 3. Comparisons of measured (filled circles) and theoretical (open circles) frequency distributions for 200 olivine–sulfide melt apparent angles measured in experiments 72 hours in duration at log f_{O_2} conditions from −9.5 to −7.9 and log f_{S_2} conditions from −2.5 to −1.5 at 1350ºC (Table 1). Theoretical distributions and best match between theoretical and observed distributions were calculated as in Fig. 2. Bin size is 10º.

relative to the theoretical one due to the existence of a range of true dihedral angles [27], and this is apparent in some of our results (e.g., Fig. 2).

3. Experimental results

The melts produced in our experiments consist dominantly of Fe, S, and O, with minor amounts of Ni, Mn, and Cr derived from the olivine starting material (Table 2). The concentration of O dissolved in the melt increases systematically from 0.09 ± 0.03 wt% at log $f_{O_2} = -9.5$ and log $f_{S_2} = -1.5$ to 8.6 ± 0.6 wt% at log $f_{O_2} = -7.9$ and log $f_{S_2} = -2.5$. Olivine grains are anhedral to subhedral (Fig. 4), with compositions ranging from $Fo_{89.0}$ to $Fo_{94.8}$ (Table 3). The Fo content of the olivine initially decreases then increases with increasing f_{O_2}/f_{S_2} ratio. An increase in the Fo content of the olivine relative to the starting material ($Fo_{90.6}$) was accommodated

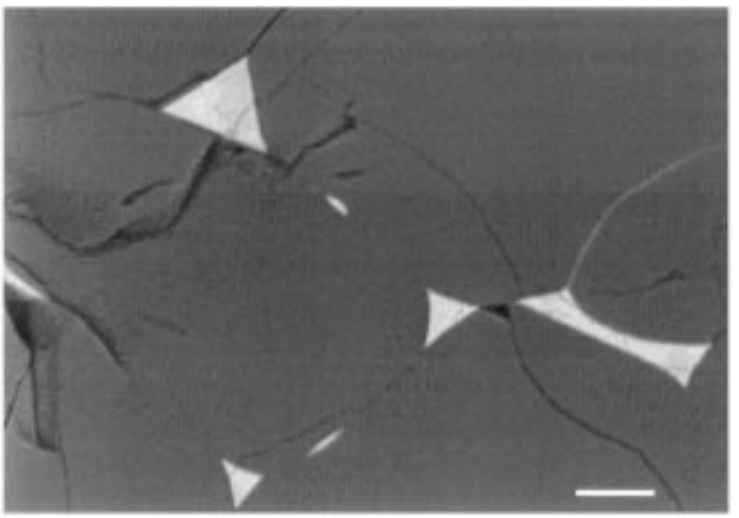

Fig. 4. Back-scattered electron image of experiment FeS-6, in which the olivine–sulfide melt dihedral angle was determined to be 52 ± 1.4^{o}. Dark grains are $Fo_{89.8}$ olivine and the light phase is sulfide melt containing 8.6 ± 0.6 wt% O. Scale bar is 10 μm.

through the orthopyroxene-forming reaction:

$$Fe_2SiO_4 + \tfrac{1}{2}S_2 = FeS + FeSiO_3 + \tfrac{1}{2}O_2 \quad (1)$$

A decrease in the Fo content of the olivine resulted in the crystallization of magnesioferrite through the reaction:

$$Mg_2SiO_4 + 6FeS + 4O_2 = Fe_2SiO_4 + 2MgFe_2O_4 + 3S_2 \quad (2)$$

Olivine–sulfide melt dihedral angles determined from our experiments range from 90 ± 2^{o} at low f_{O_2}/f_{S_2} ratio conditions to 52 ± 1^{o} at higher f_{O_2}/f_{S_2} ratio conditions (Table 4). The dihedral angles determined from short (24 hr) and long (216 hr) duration experiments do not differ significantly, indicating that a close approach to textural equilibrium is achieved in 24 hours or less (Tables 1 and 4). The agreement between the measured distribution of apparent angles and the theoretical distribution improves with increasing experiment duration, however, as the microstructure matures (Fig. 2). Therefore, although there is no significant change in dihedral angle true textural equilibrium was not achieved in the short duration experiments. One interpretation of this observation is that equilibrium dihedral an-

Table 3
Electron microprobe analyses of experimentally produced olivines

Experiment	SiO_2	TiO_2	Al_2O_3	Cr_2O_3	FeO	MnO	MgO	CaO	NiO	Total	Fo
San Carlos	40.73 (12)	0.01 (1)	0.07 (2)	0.07 (2)	9.09 (16)	0.14 (4)	49.36 (12)	0.09 (1)	0.33 (2)	99.89	0.906
FeS-4	42.2 (2)	0.01 (1)	0.03 (3)	0.06 (3)	5.38 (14)	0.05 (2)	53.1 (5)	0.07 (1)	0.03 (3)	100.93	0.946
FeS-7	41.5 (2)	0.01 (1)	0.00 (0)	0.08 (2)	5.38 (18)	0.08 (3)	53.8 (4)	0.07 (2)	0.04 (4)	100.96	0.947
FeS-1	42.1 (3)	–	0.03 (2)	0.03 (1)	5.29 (14)	0.06 (2)	53.24 (16)	0.07 (1)	0.04 (2)	100.86	0.947
FeS-3	41.7 (2)	0.03 (1)	0.02 (1)	0.11 (2)	5.26 (13)	0.07 (2)	53.8 (2)	0.08 (2)	0.08 (2)	101.15	0.948
FeS-14	41.2 (3)	0.00 (0)	0.08 (2)	0.05 (2)	9.06 (9)	0.13 (4)	50.2 (4)	0.09 (1)	0.02 (2)	100.83	0.908
FeS-9	40.4 (2)	0.05 (4)	0.06 (3)	0.09 (3)	10.43 (11)	0.11 (4)	49.3 (3)	0.04 (4)	0.03 (5)	100.51	0.894
FeS-13	40.4 (2)	0.01 (1)	0.04 (7)	0.07 (2)	10.7 (3)	0.00 (0)	48.7 (2)	0.09 (2)	0.05 (4)	100.06	0.890
FeS-6	41.0 (2)	0.01 (2)	0.03 (2)	0.10 (3)	10.0 (6)	0.09 (2)	49.6 (7)	0.06 (2)	0.10 (4)	100.99	0.898

Analyses are reported in weight percent. Fo is the molar Mg/(Mg + Fe) ratio of the olivine. Each reported analysis represents the mean of 10 spot analyses. Units in parentheses as in Table 2.

Table 4
Experimentally determined dihedral angles

	FeS-4	FeS-7	FeS-1	FeS-3	FeS-14	FeS-9	FeS-13	FeS-6
θ_M	90	90	85	90	81	72	59	52
σ	2.0	1.9	1.5	1.7	1.6	1.7	1.6	1.4

θ_M = median of 200 apparent angle measurements. σ = dihedral angle uncertainty calculated using the method of Riegger and Van Vlack [26] and reported in degrees.

gles are established relatively quickly, and that as the overall microstructure matures apparent angle measurements become more precise.

4. Discussion

4.1. Influence of dissolved oxygen on olivine–sulfide melt dihedral angles

At a given temperature and pressure, the composition of a sulfide melt is controlled primarily by the ambient f_{O_2} and f_{S_2} conditions. An example of this is given in Fig. 5, where f_{O_2} and f_{S_2} contours have been superimposed on a portion of the Fe–S–O system at 1 bar and 1200ºC [28]. At low values of f_{O_2} and f_{S_2}, (i.e., reducing conditions) metal coexists with relatively anion-poor liquids, governed by the equilibria:

$$Fe^{Metal} + \tfrac{1}{2}O_2^{Gas} = FeO^{Sulfide\ Melt} \quad (3)$$

and:

$$Fe^{Metal} + \tfrac{1}{2}S_2^{Gas} = FeO^{Sulfide\ Melt} \quad (4)$$

Because the inner core of the Earth is thought to be composed of solid FeNi metal [29], and the outer core of a metallic liquid containing ~10% light elements such as S, O, or C [13,14,30,31], it is

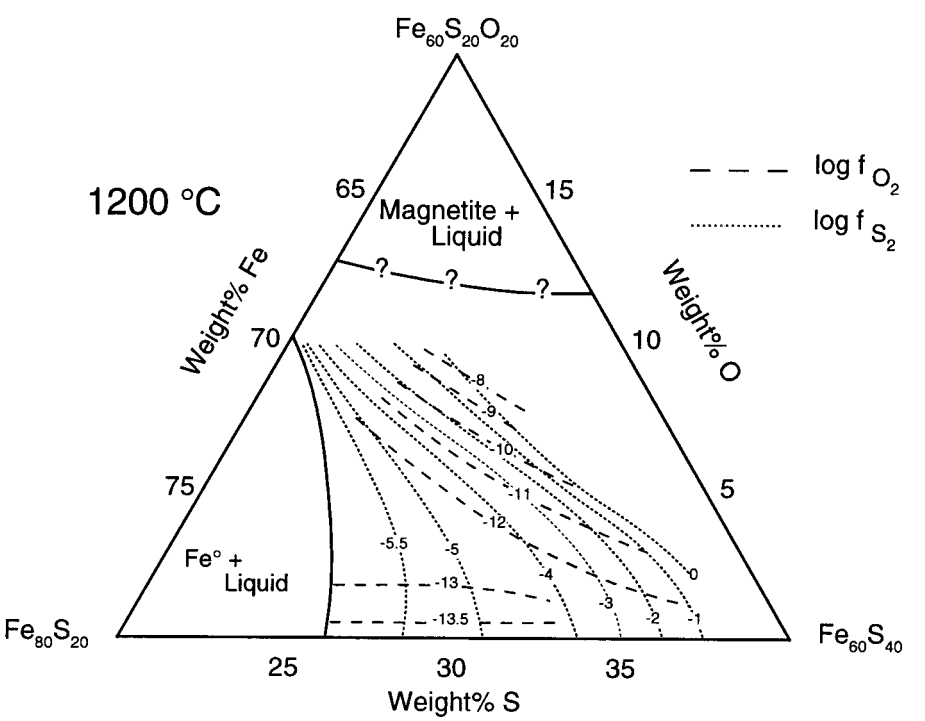

Fig. 5. Contours of constant f_{O_2} (dashes) and f_{S_2} (dots) superimposed on a portion of the system Fe–S–O at 1 bar and 1200ºC illustrating the relationship between f_{O_2} and f_{S_2} conditions and sulfide melt composition. After Shima and Naldrett [28].

commonly assumed that ambient conditions during core formation were reducing. The f_{O_2} is thought to have been below the iron–wüstite (IW) oxygen buffer and, given the low concentration of light elements in the outer core, it is probable that the f_{S_2} was also relatively low.

The ambient f_{O_2} and f_{S_2} conditions of the upper mantle are thought to have changed significantly since core formation. Estimates of modern mantle f_{O_2} from the Fe^{3+}/Fe^{2+} ratios of mid-ocean ridge basalt (MORB) glasses are commonly at or slightly below the fayalite–magnetite–quartz (FMQ) oxygen buffer [32]. Estimates of mantle f_{S_2} from the compositions of sulfides in peridotite xenoliths indicate conditions that are ~2 log units above the FeFeS buffer at an f_{O_2} 1 log unit below FMQ and 1200°C [33]. Similar f_{S_2} conditions are indicated by estimates based on the compositions of the sulfide globules in MORB glasses [10]. Further, the S (26–35 wt%) and O (2–14 wt%) contents of sulfide globules reported by Roy-Barman et al. [34] are comparable to those of our sulfide liquids (26–37 wt% S; 3–9 wt% O) produced experimentally at ~2 log units above FeFeS and 1 log unit below FMQ (Fig. 6). At these oxidizing, high sulfur fugacity conditions sulfide liquids are anion-rich, and the concentration of dissolved O varies as a function of the f_{S_2}/f_{O_2} ratio, governed by the equilibrium:

$$Fe_{1-X}S^{\text{Sulfide Melt}} + \tfrac{1}{2}O_2^{\text{Gas}} = Fe_{1-X}O^{\text{Sulfide Melt}} + \tfrac{1}{2}S_2^{\text{Gas}} \quad (5)$$

An f_{O_2} increase at constant f_{S_2} shifts reaction 5 to the right, resulting in a larger $Fe_{1-X}O$ component in the melt. The apparent anion excess in these liquids may reflect the presence of Fe^{3+} [23].

Our experimental results demonstrate that the olivine–melt dihedral angle decreases significantly as the concentration of O dissolved in an anion-rich sulfide melt increases. The experimentally determined relationships among dihedral angle, f_{O_2}/f_{S_2} ratio, and the logarithm of the mole fraction of the $Fe_{1-X}O$ component in the melt ($\log X^{\text{Sulfide Melt}}_{Fe_{1-X}O}$) are shown in Fig. 7a. In the experiments conducted at the lowest f_{O_2}/f_{S_2} ratio conditions, the melt is composed dominantly of $Fe_{1-X}S$, and the large interfacial energy between olivine and melt of this composition is demonstrated by a dihedral angle of ~90° (Table 4; Figs. 2 and 7). With an increase of the f_{O_2}/f_{S_2} ratio, and increasing dissolved O, the dihedral angle

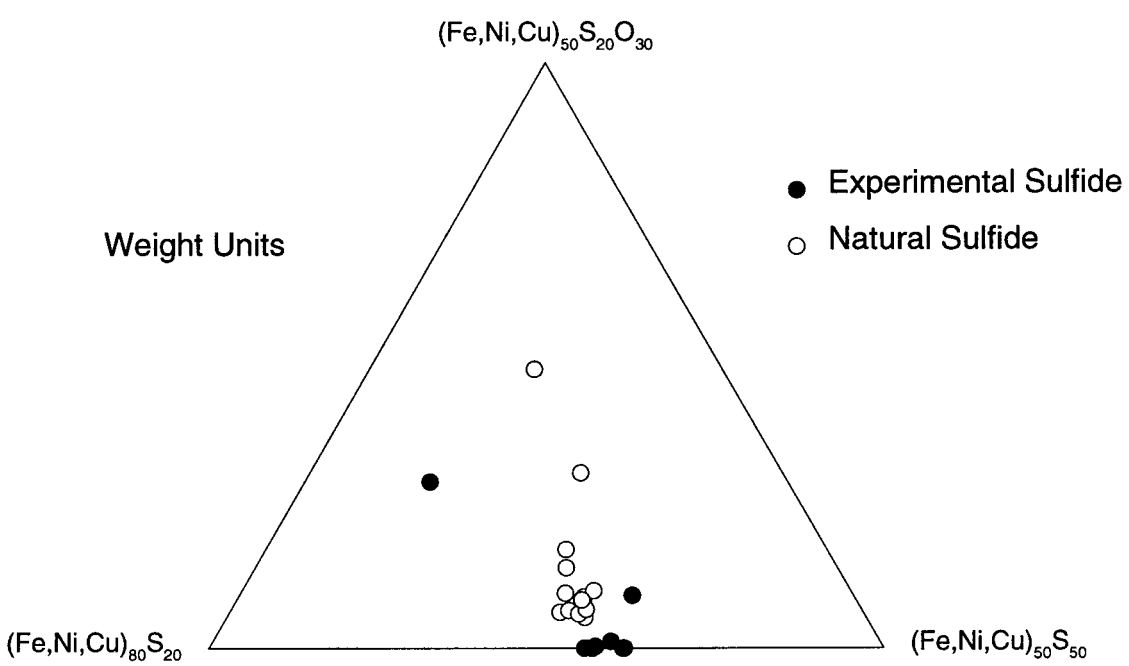

Fig. 6. A portion of the (Fe + Ni + Cu)–O–S ternary comparing the compositions of sulfide melts produced experimentally in this study with those of natural sulfide globules from MORB and Loihi glasses [34].

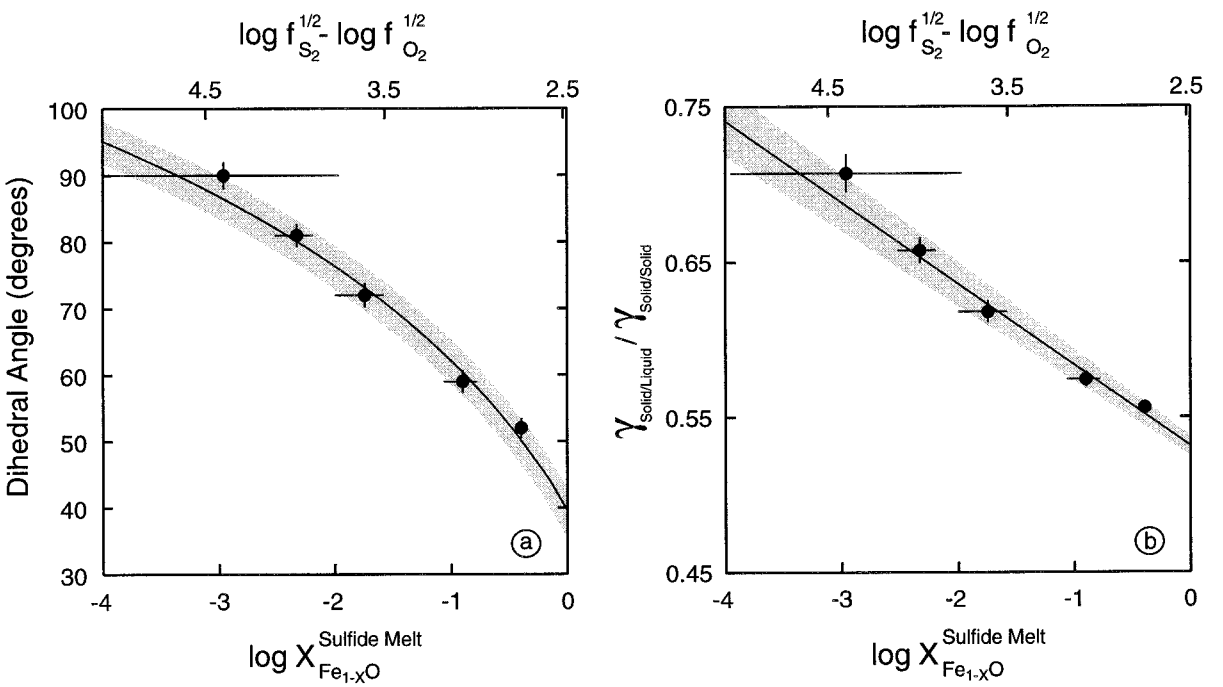

Fig. 7. (a) Plot illustrating the experimentally determined relationships among dihedral angle, the logarithm of the mole fraction of $Fe_{1-X}O$ component in the sulfide melt, and $\log f_{S_2}^{1/2} - \log f_{O_2}^{1/2}$. Solid curve shows the result from linear regression of $\gamma_{solid/liquid}/\gamma_{solid/solid}$ vs. $\log X_{Fe_{1-X}O}^{Sulfide\ Melt}$ that has been transformed into dihedral angles using the relationship $\gamma_{solid/solid}/\gamma_{solid/liquid} = 2\cos(\theta/2)$. Error bars are 1σ. The $Fe_{1-X}O$ content of the highest $\log f_{S_2}^{1/2} - \log f_{O_2}^{1/2}$ experiment was estimated using a linear regression of $\log X_{Fe_{1-X}O}^{Sulfide\ Melt}$ vs. $\log f_{S_2}^{1/2} - \log f_{O_2}^{1/2}$ for the other four experiments, and error bars were calculated using the regression parameter uncertainties. Shaded region represents 1σ uncertainties on $\gamma_{solid/liquid}/\gamma_{solid/solid}$ vs. $\log X_{Fe_{1-X}O}^{Sulfide\ Melt}$ regression parameters transformed into dihedral angles as described above. (b) Plot illustrating the experimentally determined relationships among $\gamma_{solid/liquid}/\gamma_{solid/solid}$, the logarithm of the mole fraction of $Fe_{1-X}O$ component in the sulfide melt, and $\log f_{S_2}^{1/2} - \log f_{O_2}^{1/2}$. The $\gamma_{solid/liquid}/\gamma_{solid/solid}$ ratio for each experiment was calculated from the dihedral angle determination using the relationship given above. Solid line shows the result from a linear regression of $\gamma_{solid/liquid}/\gamma_{solid/solid}$ vs. $\log X_{Fe_{1-X}O}^{Sulfide\ Melt}$ for the four experiments with measured O contents. Uncertainties are as in (a).

decreases systematically to a value of 59 ± 1.6^{o} for a melt containing 2.7 ± 0.9 wt% O, a result nearly identical to the olivine–sulfide melt dihedral angle of 60° reported by Minarik et al. [17] for a melt containing 2.9 ± 0.3 wt% O at 3.9 GPa and 1500°C. In our highest f_{O_2}/f_{S_2} ratio experiment the sulfide melt contains 8.6 ± 0.6 wt% O and the dihedral angle is 52 ± 1.4^{o} (Tables 2 and 4; Figs. 3, 4 and 7a).

The influence of O dissolved in the melt on dihedral angle can be understood by considering the nature of the interface between the coexisting phases. The excess free energy associated with a crystal surface results from the presence of atoms on that surface that are not surrounded by the same periodic arrangement that characterizes the internal structure of the crystal, resulting in unsatisfied bonds [35]. The excess free energy that characterizes a crystal–melt interface is a reflection of the suitability of the melt's constituent components for satisfying the bonds on the surface of the crystal. The minerals that make up the Earth's mantle are composed of a matrix of oxygen anions bonded to interstitial cations. The interfacial energy between these O-rich minerals and a melt composed dominantly of the components $Fe_{1-X}S$ and Fe^{o} (i.e., an oxygen-poor melt with anion/cation <1) is large because the melt components do not readily satisfy cation-oxygen bonds and, therefore, wetting of the solid grains is not energetically favored. As the O content of the melt increases, however, the bonds at the surface of these crystals are more easily satisfied by the increased $Fe_{1-X}O$ component, leading to a reduction

of the excess free energy associated with the crystal–melt interface.

The dependence of solid–melt interfacial energy on composition is a reflection of the thermodynamic relationship between interfacial energy and the chemical potential of surface-active components in the system. For a binary system, this relationship is given by the Gibbs adsorption isotherm:

$$\partial\gamma = -RT\Gamma_i \partial \log_{10} X_i \quad (6)$$

where γ is the interfacial energy, Γ_i is the excess concentration of the surface-active component at the interface, and X_i is the mole fraction of the surface-active component in one of the phases [36]. If the interfacial energy decreases with an increase in one of the components at constant pressure and temperature, there is a linear relationship between the interfacial energy and the logarithm of the mole fraction of that component. The slope of the line is proportional to the excess concentration of the component at the interface and will, therefore, be negative for components that lead to a decrease in the interfacial energy. The ratio of the solid–melt to solid–solid interfacial energies in our experiments decreases linearly with an increase in $\log X_{Fe_{1-x}O}^{\text{Sulfide Melt}}$ (Fig. 7b). Assuming that the solid–solid interfacial energy does not change significantly, this trend indicates that $Fe_{1-x}O$ (or O) is the surface active component leading to a reduction in the solid–melt interfacial energy and, thus, the dihedral angle.

Among the other variables that may affect the distribution of sulfide melt in olivine-rich rocks are pressure, temperature, and the concentrations of Ni and Cu in the melt. The experiments presented in this study were designed to isolate the effects of dissolved O on dihedral angles, so that the effects of these other variables could not be directly determined. Existing experimental data allow for an evaluation of their effects. Fig. 8a is a plot of $\log X_{Fe_{1-x}O}^{\text{Sulfide Melt}}$ versus dihedral angle comparing our experimental results with those of Minarik et al. [17], who determined olivine–sulfide liquid dihedral angles at 35 to 110 kbar and 1500°C. The dihedral angles determined by Minarik et al. [17] are systematically larger than ours, and do not show the same dependence on $\log X_{Fe_{1-x}O}^{\text{Sulfide Melt}}$. This may reflect the effects of pressure, temperature, or melt composition. The effects of pressure and temperature have

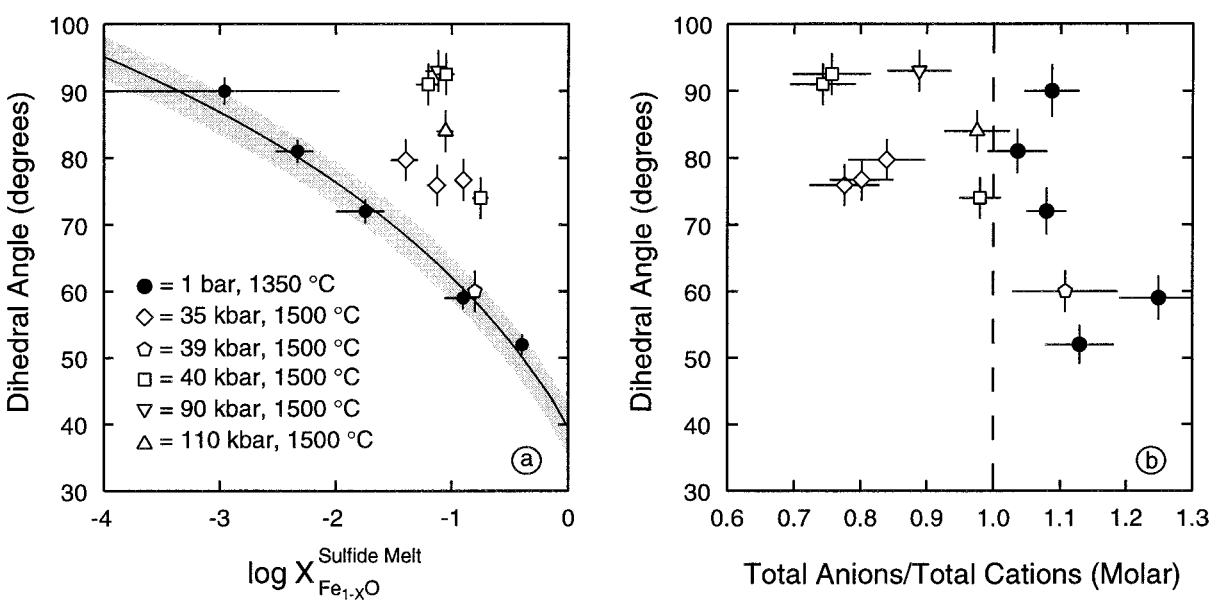

Fig. 8. (a) Plot comparing the experimentally determined relationship between dihedral angle and $\log X_{Fe_{1-x}O}^{\text{Sulfide Melt}}$ for the melts produced in this study at 1 bar (filled symbols) with that for the high-pressure melts reported by Minarik et al. [17] (open symbols). Uncertainties are as in Fig. 7b. (b) Plot of anion/cation ratio vs. dihedral angle comparing sulfide liquids produced in this study with those reported by Minarik et al. [17]. Symbols and uncertainties are as in (a).

been investigated in two previous studies. The experimental results of Shannon and Agee [19] indicate that mantle mineral–sulfide melt dihedral angles for anion-poor melts remain at ~108° from 20 kbar and 1210°C up to 200 kbar and 1710°C. Ballhaus and Ellis [18] found that olivine–Fe–Ni–Co–S liquid dihedral angles for relatively anion-rich liquids tend to decrease as temperature increases from 1350°C to 1570°C at 20 kbar, but that the effect is relatively small (~10°). Therefore, the most plausible explanation for the difference between our experimental result and that of Minarik et al. [17] is that it reflects the lower anion content of the high-pressure liquids (Fig. 8b). It is unlikely to be explicable in terms of pressure and temperature effects. This conclusion is supported by the one anion-rich liquid produced by Minarik et al. [17] at 39 kbar and 1500°C, which falls on the dihedral angle–log $X_{Fe_{1-x}O}^{Sulfide\ Melt}$ trend defined by our 1 bar experiments (pentagon in Fig. 8a, b), even though it has significantly higher Ni (13.4 ± 1.3 versus 1.3 ± 0.3 wt%).

Therefore, we agree with the conclusion of Minarik et al. [17] that the total anion content of the melt is the important compositional variable for controlling olivine–sulfide liquid dihedral angles *for anion-poor melt*. Our experimental results indicate, however, that for anion-rich melt the concentration of dissolved O is the controlling factor. Although additional work is needed, pressure and temperature appear to be secondary to sulfide liquid composition in controlling the distribution of sulfide melt in olivine-rich rocks.

4.2. Mobility of sulfide melt in upper mantle peridotite

Olivine–sulfide melt dihedral angles of 60° or less indicate that percolation of sulfide could occur in the upper mantle. There are a number of factors that might inhibit porous flow, however, including the low permeability implied by the limited amount of sulfide in fertile peridotite (~0.1 wt% or less). McKenzie [37] considered the mobility of small amounts of melt (≤1%) in mantle rocks, and concluded that only 10^{-3}% melt is necessary for segregation if the melt viscosity (μ) is as low as 0.1 Pa s, and the matrix-melt density contrast ($\Delta\rho$) is at least 10^3 kg/m^3. Sulfide melt is less viscous ($\mu \sim 0.002$ Pa s) than the liquids modeled by McKenzie [37], with a significantly greater peridotite-melt density contrast ($\Delta\rho \sim 2 \times 10^3$ kg/m^3) so that, in theory, even very small amounts of melt should segregate. The velocity of melt percolation driven by a matrix-melt density contrast is given by:

$$V = \frac{\Delta\rho \times g \times k}{\mu} \quad (7)$$

where g is the acceleration due to gravity and k is the permeability of the matrix [38]. Although there are considerable uncertainties associated with both μ and k, Eq. 7 can be used to quantitatively estimate the efficiency of sulfide melt migration. The melt velocity calculated for a grain diameter, d, of 1 mm using the permeability–porosity relationship determined experimentally by Wark and Watson [39]:

$$k = \frac{d^2\phi^3}{200} \quad (8)$$

is ~2 mm/yr. At this velocity sulfide melt would require ~1.5 billion years to percolate from the shallow mantle to the core. This may represent a minimum velocity, however, as the relationship between porosity and permeability may change at very low melt fractions, where both Wark and Watson [39] and Minarik and Watson [40] found evidence for enhanced permeability. An additional complication is that the efficiency of sulfide transport through the mantle is likely to change as a function of depth, due to the effects of pressure and temperature on both $\Delta\rho$ and μ.

4.3. Sulfide melt as a metasomatic agent in the Earth's upper mantle

The presence of sulfide melt in the upper mantle is commonly used to explain chalcophile element fractionations associated with peridotite partial melting [41–44]. Due to its relatively low melting point, Fe–Ni–Cu–S–O sulfide will be molten at temperatures below the anhydrous peridotite solidus. The potential mobility of sulfide melt indicates that it may act as a metasomatic agent in mantle peridotite at these conditions, producing some of the trace element and isotopic heterogeneity found in upper mantle materials [45–47]. The O contents of sulfide globules in MORB and in Loihi glasses are comparable to

Table 5
Sulfide melt–olivine partition coefficients used for trace element calculations

D_{Re}	D_{Os}	D_{U}	D_{Th}	D_{Pb}
2.7	3.7×10^4	130	332	2000

Partition coefficients were adopted on the basis of Murrell and Burnett [48], Meijer et al. [49], and Burton et al. [50].

the concentration required to achieve connectivity (Fig. 6), an indication that modern basalt source regions may span the range of f_{O_2} and f_{S_2} conditions over which sulfide melt connectivity is achieved. There may be regions of the mantle in which the f_{O_2}/f_{S_2} ratio is too small for connectivity at low melt fractions, producing zones where migrating sulfide becomes stranded until conditions change or the concentration of sulfide melt becomes large enough that an interconnected network is reestablished. Although sulfide may be lost due to porous flow, it is being recycled back into the mantle through the subduction of ocean-floor massive sulfide deposits.

In the Re/Os, U/Pb, and Th/Pb isotopic systems, the radiogenic daughter In products are significantly more chalcophile than their parents, and the addition or removal of relatively small amounts of sulfide melt will fractionate parent/daughter ratios in mantle rocks. Over time these fractionations would be reflected in the isotopic compositions of Os and Pb. Sulfide percolation may also produce variations in the absolute and relative abundances of the platinum group elements (PGE). Given the importance of interpretations of the isotopic compositions of Os and Pb for understanding mantle evolution, we adopted a set of sulfide melt–olivine partition coefficients on the basis of the work of Murrell and Burnett [48], Meijer et al. [49], and Burton et al. [50] (Table 5), and used them to determine the sensitivity of peridotite Re/Os, U/Pb, and Th/Pb ratios to sulfide metasomatism.

Fig. 9 contains plots of normalized parent/daughter ratios versus weight percent sulfide removed from mantle peridotite via porous flow. Although there is uncertainty surrounding the sulfur content of fertile mantle peridotite, the upper limit on the amount of sulfide melt present is probably on the order of 0.1 wt% [51], and is shown by dashed lines in Fig. 9. The Re/Os fractionation that can be produced by the removal of as little as 0.01 wt% sulfide is substantial, and has the potential to produce highly radiogenic Os in mantle-derived rocks. An increase in the Re/Os ratio due to removal of sulfide melt is opposite to the fractionation produced by partial melting, and may produce anomalous Re depletion or model ages.

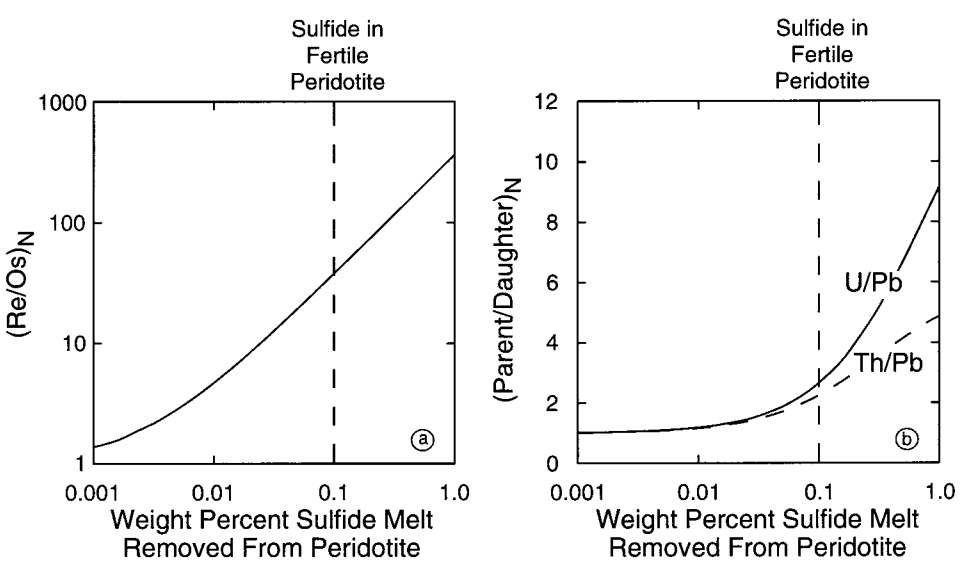

Fig. 9. Plot of (a) Re/Os and (b) U/Pb and Th/Pb ratios vs. weight percent sulfide removed from mantle peridotite via porous flow. All ratios have been normalized to an arbitrary initial ratio for clarity. Dashed line represents an estimate for the wt% sulfide melt in a fertile peridotite [51]. Partition coefficients used in the calculations are listed in Table 5.

That highly radiogenic Os is not common in mantle rocks may indicate that percolation of sulfide melt is only important under a limited set of conditions, or that the difference in the olivine–sulfide melt partition coefficients for Re and Os are not as large as inferred from the data we used to calculate the partition coefficients in Table 5. The addition of sulfide melt to mantle peridotite will decrease the Re/Os ratio and, because sulfide is the primary host for Os [11], may produce substantial changes in the Os isotopic composition of the whole rock. This process could also complicate our understanding of the Re/Os system in mantle peridotite and lead to incorrect interpretations of Os isotopic compositions. In contrast, the U/Pb and Th/Pb systems require the addition or removal of relatively large amounts of sulfide melt to significantly fractionate parent/daughter ratios. Nearly all of the sulfide melt must be extracted from a fertile peridotite in order to increase the U/Pb or Th/Pb ratios of the whole rock by a factor of two.

There is evidence from both orogenic lherzolites and peridotite xenoliths to indicate that sulfide melt is mobile in mantle rocks, and that this mobility produces significant changes in the absolute and relative abundances of the PGE and in the isotopic composition of Os. Garuti et al. [52] reported enrichments in Au and PGE in peridotites from the Ivrea Zone in the Italian western Alps. These enrichments are spatially associated with basaltic dikes, but interelemental correlations indicate that the metals were introduced into the peridotite by infiltration of sulfide melt. Pearson et al. [53] noted that the $^{187}Re/^{188}Os$ ratios of peridotite xenoliths from the Kaapvaal craton give anomalous model ages, but do not correlate with any of the highly incompatible elements. Such a correlation would be expected if the Re/Os ratio of the peridotite had been reset by infiltration of a silicate melt. One possible explanation for these anomalous Re/Os ratios is sulfide metasomatism. There is also evidence for the addition of radiogenic Os by sulfide infiltration in peridotite xenoliths from Tanzania [54]. In this case the radiogenic Os is a product of its relatively high concentration in mantle sulfide rather than parent/daughter fractionations produced by sulfide infiltration. Further work is needed to determine the extent of sulfide metasomatism in the mantle, and its effects on chalcophile element abundances.

4.4. Mobility of sulfide melt during accretion of the Earth

The results from this study provide constraints on possible mechanisms for core formation in the early Earth. Most core formation models involve accretion of a mixture of silicates and metal, followed by the segregation of dense, Fe-rich material to form the core [55–57]. Catastrophic core formation, in which emplacement and growth of the Earth's protocore occurred during the later stages of accretion through the migration of FeNi metal (± S, O) downward in fractures or as negatively-buoyant diapirs [55–57], would have released enough gravitational energy to raise the temperature of the Earth by 2000°C, resulting in large-scale melting of the silicate mantle [58,59]. Once the silicate portion of the Earth was molten, additional core-forming material may have segregated as immiscible droplets [15,16,57].

An alternative to catastrophic core formation is that, due to the melting-point lowering effect of light alloying elements on metallic Fe, some or all of the core-forming material was molten and that porous flow in the mantle allowed the core to grow continuously throughout accretion. Continuous core formation would have released gravitational energy more gradually, lessening the thermal effects. Estimates for the amount of S and/or O required to explain the density of the liquid outer core are ~9–11 wt% [60]. Here we consider the implications of our experimental results for the mobility of core-forming melts during heterogeneous accretion, in which the oxidation state of the material added to the early Earth increased as accretion proceeded. We first discuss the implications for heterogeneous accretion models in which the composition of accreting material changes gradually, then for a model in which oxidized material is added to the Earth during a Moon-forming giant impact.

In most heterogeneous accretion models, ~80 to 85% of the mass of the Earth is formed from reduced material resembling a high-temperature nebular condensate [61,62]. Our experimental results, as well as those from previous studies [17–19], indicate that sulfide melt would only have been interconnected in a reduced proto-Earth at relatively large melt fractions. If segregation of core-forming material did occur by porous flow, connectivity would have been

transient, with ~6 vol% melt remaining in isolated pockets in the mantle [2]. This amount of trapped melt is more than twice that predicted by the inefficient core formation model of Jones and Drake [63] (~3 vol%), and would have resulted in an upper mantle with siderophile element and S abundances in excess of the measured concentrations.

As accretion proceeded, however, and oxidized material was mixed into the mantle, the S and O content of sulfide melt would have increased. If f_{O_2} and f_{S_2} conditions comparable to estimates for the present-day upper mantle were achieved [10,32,33], sulfide melt could have formed an interconnected network in peridotite down to very low melt fractions. This implies that porous flow may have been an important mechanism for segregating sulfide melt from the final 15–20% of the material accreted to the Earth. Further, melt trapped during the early stages of accretion may have been remobilized as the ambient oxidation state of the mantle increased. Determinations of dihedral angles between anion-poor sulfide melt and the phases that make up the lower mantle indicate that they are significantly smaller than for the phases that constitute the upper mantle (~71° versus ~108°) [64]. The effect on interfacial energies of increasing the O content of the liquid is likely to be similar for lower mantle phases and olivine, in which case sulfide melt could percolate efficiently from the upper mantle, through the lower mantle, and into the core.

If this mechanism for segregation of core-forming material during late-stage accretion is correct, it is debatable whether the addition of a chondritic veneer to the Earth following formation of the core is a viable explanation for the apparent over-abundance of highly siderophile elements in the upper mantle [62,65]. Even if this material were initially reduced, it would have equilibrated at more oxidizing conditions as it was mixed into the upper mantle. Sulfide melt would have segregated from the silicate matrix by porous flow, carrying a significant proportion of the highly siderophile elements added by the late veneer.

O'Neill [66] proposed an alternative type of heterogeneous accretion model in which ~90% of the mass of the Earth was accreted from reduced material. During or just after accretion, segregation of Fe-rich metal formed a core and stripped the early mantle of elements more siderophile than Fe. A Moon-forming giant impact added oxidized material to the Earth, bringing it to ~99% of its present mass and raising the oxidation state of the mantle close to the FMQ buffer. O'Neill [66] surmised that at these conditions sulfide liquid (or "Hadean matte") would be rich enough in O to wet mantle olivine, allowing percolation into the core. Segregation of 0.2 wt% sulfide melt at oxidizing conditions established the concentrations of the moderately siderophile elements, and transported the highly siderophile elements to the core. The observed concentrations of the highly siderophile elements were then established by a veneer of reduced chondritic material added to the mantle following extraction of the Hadean matte.

Our experimental results confirm O'Neill's [66] contention that an O-rich Hadean matte could have segregated from the mantle into the core by porous flow. Further, the experiments of Gaetani and Grove [12] provide low-pressure sulfide melt-olivine partition coefficients at f_{O_2} and f_{S_2} conditions appropriate for calculating the effect of matte extraction on the abundances of moderately siderophile elements in the upper mantle of the Earth. Fig. 10 shows the results from these calculations for the first series

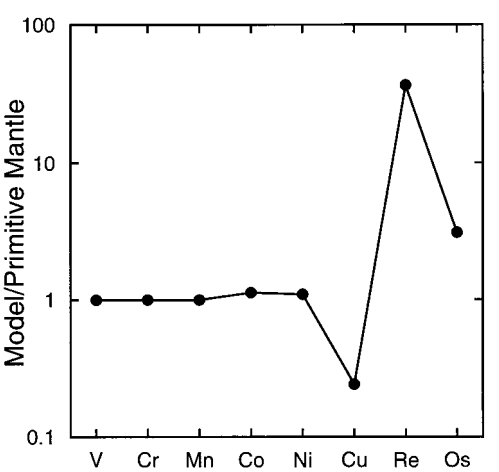

Fig. 10. Plot showing primitive mantle normalized siderophile element abundances calculated for the heterogeneous accretion model of O'Neill [66] using sulfide melt–olivine partition coefficients from the experiments of Gaetani and Grove [12] carried out at 1 bar and 1350°C with log $f_{O_2} = -7.9$ and log $f_{S_2} = -1.8$ ($D_V = 0.19$; $D_{Cr} = 0.12$; $D_{Mn} = 0.06$; $D_{Co} = 9$; $D_{Ni} = 70$; $D_{Cu} = 2800$) or from Table 5. Primitive mantle abundances were taken from O'Neill [66] and references therein.

transition metals V through Cu, as well as Re and Os. The calculated abundances of the moderately siderophile elements are within 13% of primitive mantle concentrations except for Cu which, at 5 ppm, is significantly more depleted than even the 21 ppm concentration advocated by O'Neill [66]. In addition to the strong Cu depletion, matte extraction would have produced a strongly superchondritic Re/Os ratio if the sulfide melt–olivine partition coefficients listed in Table 5 are appropriate. Therefore, although our wetting angle results are consistent with O'Neill's [66] heterogeneous accretion model, low pressure sulfide melt–olivine partitioning at relatively oxidizing conditions does not produce the required mantle siderophile element abundance pattern.

Acknowledgements

The authors thank J. Jones, E. Mathez, and W. Minarik for insightful and constructive reviews. We are also grateful to P. Asimow, S. Bowring, F. Frey, P. Hess, A. Holzheid, M. Humayun, K. Righter, and R. Rudnick for commenting on the manuscript. We thank G. Hirth for reading an early version of the paper and for providing advice and encouragement over the course of the study. E.B. Watson provided helpful discussions and suggestions. K. Koga furnished the software used to calculate theoretical apparent angle distributions. W. Minarik generously supplied unpublished data. The first author gratefully acknowledges the financial support of E.M. Stolper and E.B. Watson during final manuscript preparation. This work was supported by NASA grant NAGW-3586. ***[CL]***

References

[1] C.S. Smith, Some elementary principles of polycrystalline microstructure, Metall. Rev. 9 (1964) 1–48.
[2] N. von Bargen, H.S. Waff, Permeabilities, interfacial areas and curvatures of partially molten systems: Results of numerical computations of equilibrium microstructures, J. Geophys. Res. 91 (1986) 9261–9276.
[3] J.G. Moore, L.C. Calk, Sulfide spherules in vesicles of dredged pillow basalt, Am. Mineral. 56 (1971) 476–488.
[4] E.A. Mathez, Sulfur solubility and magmatic sulfides in submarine basalt glass, J. Geophys. Res. 81 (1976) 4269–4275.
[5] G.K. Czamanske, J.G. Moore, Composition and phase chemistry of sulfide globules in basalt from the Mid-Atlantic Ridge rift valley near 37ºN Lat, Geol. Soc. Am. Bull. 88 (1977) 587–599.
[6] E.M. Dromgoole, J.D. Pasteris, Interpretation of the sulfide assemblages in a suite of xenoliths from Kilbourne Hole, New Mexico, in: E.M. Morris, J.D. Pasteris (Eds.), Mantle Metasomatism and Alkaline Magmatism, Geological Society of America, Boulder, CO, Geol. Soc. Am. Spec. Pap. 215 (1987) 25–46.
[7] G. Garuti, C. Gorgoni, G.P. Sighinolfi, Sulfide mineralogy and chalcophile and siderophile element abundances in the Ivrea-Verbano mantle peridotites (Western Italian Alps), Earth Planet. Sci. Lett. 70 (1984) 69–87.
[8] J.P. Lorand, Sulfide petrology and sulfur geochemistry of orogenic lherzolites: A comparative study of the Pyrenean bodies (France) and the Lanzo massif (Italy), J. Petrol., Lherzolites Special Issue (1991) 77–95.
[9] C.L. Peach, E.A. Mathez, Sulfide melt–silicate melt distribution coefficients for nickel and iron and implications for the distribution of other chalcophile elements, Geochim. Cosmochim. Acta 57 (1993) 3013–3021.
[10] C.L. Peach, E.A. Mathez, R.R. Keays, S.J. Reeves, Experimentally determined sulfide melt–silicate melt partition coefficients for iridium and palladium, Chem. Geol. 117 (1994) 361–377.
[11] S.R. Hart, G.E. Ravizza, Os partitioning between phases in mantle lherzolite, in: A. Basu, S.R. Hart (Eds.), Earth Processes: Reading the Isotopic Code, American Geophysical Union, Washington D.C., Geophys. Monogr. 95 (1996) 123–134.
[12] G.A. Gaetani, T.L. Grove, Partitioning of moderately siderophile elements among olivine, silicate melt, and sulfide melt: Constraints on core formation in the Earth and Mars, Geochim. Cosmochim. Acta 61 (1997) 1829–1846.
[13] B. Mason, Composition of the Earth, Nature 211 (1966) 616–618.
[14] V.R. Murthy, H.T. Hall, The chemical composition of the Earth's core: Possibility of sulfur in the core, Phys. Earth. Planet. Inter. 2 (1970) 276–282.
[15] J. Li, C.B. Agee, Geochemistry of mantle–core differentiation at high pressure, Nature 381 (1996) 686–689.
[16] K. Righter, M.J. Drake, G. Yaxley, Prediction of siderophile element metal–silicate partition coefficients to 20 GPa and 2800 degrees C: The effects of pressure, temperature, oxygen fugacity, and silicate and metallic melt compositions, Phys. Earth. Planet. Inter. 100 (1997) 115–134.
[17] W.G. Minarik, F.J. Ryerson, E.B. Watson, Textural entrapment of core-forming melts, Science 272 (1996) 530–533.
[18] C. Ballhaus, D.J. Ellis, Mobility of core melts during Earth's accretion, Earth Planet. Sci. Lett. 143 (1996) 137–145.
[19] M.C. Shannon, C.B. Agee, High pressure constraints on percolative core formation, Geophys. Res. Lett. 23 (1996) 2717–2720.

[20] G.M. Biggar, Diopside, lithium metasilicate and the 1968 temperature scale, Mineral. Mag. 38 (1972) 768–770.
[21] K. Ehlers, T.L. Grove, T.W. Sisson, S.I. Recca, D.A. Zervas, The effect of oxygen fugacity on the partitioning of nickel and cobalt between olivine, silicate melt, and metal, Geochim. Cosmochim. Acta 56 (1992) 3733–3743.
[22] D. Walker, L. Norby, J.H. Jones, Superheating effects on metal–silicate partitioning of siderophile elements, Science 262 (1993) 1858–1861.
[23] V. Kress, Thermochemistry of sulfide liquids. I. The system O–S–Fe at 1 bar, Contrib. Mineral. Petrol. 127 (1997) 176–186.
[24] G.A. Gaetani, Experimental investigations of differentiation processes in the terrestrial planets, unpubl. Ph.D. thesis, Massachusetts Institute of Technology, 1996, 227 pp.
[25] D. Harker, E.R. Parker, Grain shape and grain growth, Trans. Am. Soc. Met. 34 (1945) 156–201.
[26] O.K. Riegger, L.H. Van Vlack, Dihedral angle measurement, Trans. Metal. Soc. AIME 218 (1960) 933–935.
[27] C.A. Stickels, E.E. Hucke, Measurement of dihedral angles, Trans. Metal. Soc. AIME 230 (1964) 795–801.
[28] H. Shima, A.J. Naldrett, Solubility of sulfur in an ultramafic melt and the relevance of the system Fe–S–O, Econ. Geol. 70 (1975) 960–967.
[29] B.R. Julian, D. Davies, R.M. Sheppard, PKJKP, Nature 235 (1972) 317–318.
[30] F. Birch, Density and composition of mantle and core, J. Geophys. Res. 69 (1964) 4377–4388.
[31] A.E. Ringwood, Composition of the core and implications for origin of the Earth, Geochem. J. 11 (1977) 111–135.
[32] D.M. Christie, I.S.E. Carmichael, C.H. Langmuir, Oxidation state of mid-ocean ridge basalt glasses, Earth Planet. Sci. Lett. 79 (1986) 397–411.
[33] D.H. Eggler, J.P. Lorand, Mantle sulfide geobarometry, Geochim. Cosmochim. Acta 57 (1993) 2213–2222.
[34] M. Roy-Barman, G.J. Wasserburg, D.A. Papanastassiou, M. Chaussidon, Osmium isotopic compositions and Re–Os concentrations in sulfide globules from basaltic glasses, Earth Planet. Sci. Lett. 154 (1998) 331–347.
[35] D.A. Porter, K.E. Easterling, Phase Transformations in Metals and Alloys, Chapman and Hall, New York, NY, 1981, 446 pp.
[36] G.W. Castellan, Physical Chemistry, Benjamin/Cummings, Reading, MA, 1983, 943 pp.
[37] D. McKenzie, Some remarks on the movement of small melt fractions in the mantle, Earth Planet. Sci. Lett. 95 (1989) 53–72.
[38] E. Stolper, D. Walker, B.H. Hager, J.F. Hays, Melt segregation from partially molten source regions: the importance of melt density and source region size, J. Geophys. Res. 86 (1981) 6261–6271.
[39] D.A. Wark, E.B. Watson, Grain-scale permeabilities of texturally equilibrated, monomineralic rocks, Earth Planet. Sci. Lett. 164 (1998) 591–605.
[40] W.G. Minarik, E.B. Watson, Interconnectivity of carbonate melt at low melt fraction, Earth Planet. Sci. Lett. 133 (1995) 423–437.
[41] C.L. Peach, E.A. Mathez, R.R. Keays, Sulfide melt–silicate melt distribution coefficients for noble metals and other chalcophile elements as deduced from MORB: Implications for partial melting, Geochim. Cosmochim. Acta 54 (1990) 3379–3389.
[42] A.N. Halliday, D.-C. Lee, S. Tommasini, G.R. Davies, C.R. Paslick, J.G. Fitton, D.E. James, Incompatible trace elements in OIB and MORB and source enrichment in the sub-oceanic mantle, Earth Planet. Sci. Lett. 133 (1995) 379–395.
[43] K. Gueddari, M. Piboule, J. Amossé, Differentiation of platinum-group elements (PGE) and of gold during partial melting of peridotites in the lherzolitic massifs of the Betico-Rifean range (Ronda and Beni Bousera), Chem. Geol. 134 (1996) 181–197.
[44] K.W.W. Sims, D.J. DePaolo, Inferences about mantle magma sources from incompatible element concentration ratios in oceanic basalts, Geochim. Cosmochim. Acta 61 (1997) 765–784.
[45] M. Tatsumoto, Isotopic composition of lead in oceanic basalt and its implication to mantle evolution, Earth Planet. Sci. Lett. 38 (1978) 63–87.
[46] K. Hattori, S.R. Hart, Osmium-isotope ratios of platinum group mineral associated with ultramafic intrusions: Os-isotopic evolution of the mantle, Earth Planet. Sci. Lett. 107 (1991) 499–514.
[47] C.E. Martin, Osmium isotopic characteristics of mantle-derived rocks, Geochim. Cosmochim. Acta 55 (1991) 1421–1434.
[48] M.T. Murrell, D.S. Burnett, Partitioning of K, U, and Th between sulfide and silicate liquids; implications for radioactive heating of planetary cores, J. Geophys. Res. 91 (1986) 8126–8136.
[49] A. Meijer, T.-T. Kwon, G.R. Tilton, U–Th–Pb partitioning behavior during partial melting in the upper mantle; implications for the origin of high mu components and the "Pb paradox", J. Geophys. Res. 95 (1990) 433–448.
[50] K.W. Burton, P. Schiano, J.-L. Birck, C.J. Allegre, The behavior of Re and Os in mantle minerals with implications for mantle melting (Abst.), Eos, Trans. Am. Geophys. Un. 79 (1998) S373.
[51] J.P. Lorand, Are spinel lherzolite xenoliths representative of the abundance of sulfur in the upper mantle?, Geochim. Cosmochim. Acta 54 (1990) 1487–1492.
[52] G. Garuti, M. Oddone, J. Torres-Ruiz, Platinum-group-element distribution in subcontinental mantle: evidence from the Ivrea Zone (Italy) and the Betic-Rifean cordillera (Spain and Morocco), Can. J. Earth Sci. 34 (1997) 444–463.
[53] D.G. Pearson, R.W. Carlson, S.B. Shirey, F.R. Boyd, P.H. Nixon, Stabilisation of Archean lithospheric mantle: A Re–Os isotope study of peridotite xenoliths from the Kaapvaal craton, Earth Planet. Sci. Lett. 134 (1995) 341–357.
[54] J.T. Chesley, R.L. Rudnick, C.-T. Lee, Re–Os systematics of mantle xenoliths from the East African Rift: evidence for longevity of cratonic mantle and Os metasomatism, Geochim. Cosmochim. Acta (in press).
[55] W.M. Elsasser, Early history of the Earth, in: J. Geiss, E.

Goldberg (Eds.), Earth Science and Meteoritics, North-Holland, Amsterdam, 1963, pp. 1–31.
[56] D.J. Stevenson, Models of the Earth's core, Science 214 (1981) 611–619.
[57] D.J. Stevenson, Fluid dynamics of core formation, in: H.E. Newsom, J.H. Jones (Eds.), Origin of the Earth, Oxford University Press, New York, NY, 1990, pp. 231–249.
[58] F. Birch, Energetics of core formation, J. Geophys. Res. 70 (1965) 6217–6221.
[59] F.M. Flaser, F. Birch, Energetics of core formation: A correction, J. Geophys. Res. 78 (1973) 6101–6103.
[60] J.-P. Poirier, Light elements in the Earth's outer core: A critical review, Phys. Earth. Planet. Inter. 85 (1994) 319–337.
[61] A.E. Ringwood, Origin of the Earth and Moon, Springer, New York, NY, 1979, 295 pp.
[62] H. Wänke, Constitution of the terrestrial planets, Philos. Trans. R. Soc. A 303 (1981) 287–302.
[63] J.H. Jones, M.J. Drake, Geochemical constraints on core formation in the Earth, Nature 322 (1986) 221–228.
[64] M.C. Shannon, C.B. Agee, Percolation of core melts at lower mantle conditions, Science 280 (1998) 1059–1061.
[65] J.W. Morgan, G.A. Wandless, R.K. Petrie, A.J. Irving, Composition of the earth's upper mantle — II: Volatile trace elements in ultramafic xenoliths, Proc. Lunar Planet. Sci. Conf. 11 (1980) 213–233.
[66] H.St.C. O'Neill, The origin of the Moon and the early history of the Earth — A chemical model. Part 2: The Earth, Geochim. Cosmochim. Acta 55 (1991) 1159–1172.